Microsyst Technol
DOI 10.1007/s00542-014-2292-7

TECHNICAL PAPER

Modeling in vitro neural electrode interface in neural cell culture medium

Tao Sun · Wei Mong Tsang · Woo-Tae Park · Kangjian Cheng · Srinivas Merugu

Received: 20 June 2014 / Accepted: 24 July 2014

Abstract A stable neural interface between neural electrodes and surrounding tissues is a critical point to achieve long-term signal recording stability, and flexible polymer-based neural microelectrodes are attracting growing interests due to their mechanical properties compatible to surrounding tissues and potential to minimize post-implantation injury. As a fundamental study to have an insight into the flexible polymer-based microelectrode–tissue interface in vivo, the neural microelectrode interface was investigated in vitro in neural cell culture medium. Flexible polyimide-based gold electrodes used for recording neural signals were micro fabricated and packaged to model the in vitro neural microelectrode–cell medium interface. The surface of gold recording sites of the neural microelectrode was observed using scanning electron microscopy (SEM), and island-like structure with the size of 537.4 ± 357.2 nm was visualized. To better understand biological processes that affect neural signal recording, the microelectrodes were immersed in neural cell culture medium for 9 days, and electrochemical impedance spectroscopy (EIS) measurement was carried out at each time point. Nyquist and Bode plots resulting from the EIS measurement were analyzed by fitting the experimental data with equivalent circuit models. On the basis of equivalent circuit models, physical processes occurring at the interface were described. Moreover, the mechanism for the impedance variation of recording sites in cell culture medium was discussed.

T. Sun (✉) · W. M. Tsang · W.-T. Park · S. Merugu
Institute of Microelectronics, Agency for Science, Technology and Research (A*STAR), Singapore, Singapore
e-mail: taosun@hotmail.com.hk; sunt@ime.a-star.edu.sg

W. M. Tsang
Hong Kong Applied Science and Technology Research Institute (ASTRI), Hong Kong, China

W.-T. Park
Department of Mechanical and Automotive Engineering, Seoul National University of Science and Technology, Seoul, Republic of Korea

K. Cheng
Department of Materials Science and Engineering, National University of Singapore, Singapore, Singapore

1 Introduction

Since the first experimental demonstration in 1999 that simultaneously recorded brain activities by neural electrodes could be used to control robotic devices, scientific community pays enormous attention to the research on neural interface, with the hope of restoring lost motor functions for paralyzed patients (Chapin et al. 1999). Compared to other non-invasive or semi-invasive approaches to record neural signals, such as electroencephalography (EEG) and electrocorticography (ECoG), neural electrode fully implanted into brain is cable of capturing high-precision neural signals which can be decoded to control the robotic devices with multiple degrees of freedom. It was reported that a tetraplegic patient was able to freely move a prosthetic limb to perform 7-dimensional movements without adverse event, after being implanted two 96-channel intracortical microelectrodes and subsequent 13 week training (Collinger et al. 2013). Moreover, recent study by Shanechi et al. demonstrated that neural activity recorded from premotor neurons by invasive multiple recording silicon multielectrode arrays could be employed to control limb movements in paralyzed primate avatars (Shanechi et al. 2014). Therefore, implanting neural electrode might be an

Published online: 09 August 2014

alternative therapy to treat patients suffering from paralysis, and the market size of the neural electrode is expected to grow dramatically.

Although being a success both in research and short-term clinical applications, fully implantable neural electrodes still face some technical challenges. First, the neural signals in the order of microvolts could be attenuated or lost due to the noisy, ion-based electric fluctuations of the surrounding cerebrospinal fluid if the microelectrode impedance is not low enough (Franks et al. 2005). Moreover, scar tissues are usually formed at the interface between conventional silicon-based electrodes and the cortical tissue, and encapsulate the microelectrode as a consequence of over-expressed foreign body responses upon the implantation, resulting in up-regulated interface impedance, instability of neural signal and failure of the microelectronics device (Rousche and Normann 1998). In addition, post-implantation injury causes health concerns due to the mismatch in mechanical properties between rigid Si-based neural electrodes and soft cortical tissues (Gilletti and Muthuswamy 2006). Therefore, it is essential to establish a stable neural interface between the neural electrode and surrounding delicate neural tissues for long-term clinical applications. Recently, flexible polymer-based microelectrodes were proposed and expected to minimize the formation of the scar tissue and post-implantation injury (Tsang et al. 2010).

To improve the efficiency and stability of neural signal recording, many scientific efforts are devoted to investigating the electrode-tissue interface. Duan et al. suggested that a reduction and composition variation of extracelluar fluid surrounding the electrode, resulting from reactive tissue responses, caused an enhanced "contact impedance" (Duan et al. 2004). To quantify the electrode–electrolyte interface impedance, Franks et al. reported that a conventional equivalent circuit model consisting of interface capacitance impedance, shunted by a charge transfer resistance, in series with the solution resistance, fit the results from electrochemical impedance spectroscopy (EIS) well (Franks et al. 2005). Furthermore, a novel model was proposed by Mercanzini et al. to describe the impedance of the scar tissue encapsulation (Mercanzini et al. 2009).

While these studies illustrate some of the recent progress in this area, the polymer-based neural microelectrode interface has not been extensively studied, especially using neural cell culture medium as the electrolyte, and there are still many fundamental and practical issues regarding the neural interface, which must be addressed to make the neural electrode a reliable technology. Low-interface impedance and accurate equivalent circuit models are crucial in designing modern microelectrode, and EIS is a sensitive and powerful technique to study the electrode interfaces where ionic transfer is dominant (Baek et al. 2011; Rui et al. 2011). As a first step to have an insight into the flexible polymer-based microelectrode–tissue interface in vivo, alternative current impedance studies were carried out at the microelectrode–electrolyte interface in vitro using EIS. To more accurately mimetic the in vivo biological processes occurring at electrode–tissue interface after implantation, neural cell culture medium was used as the electrolyte in this study. Recording sites of flexible PI-based microelectrodes were immersed in neural cell culture medium for 9 days to investigate the effect of protein encapsulation on electrical properties. At different time points (day 0, 3, 5, 7 and 9), equivalent circuit models were developed to fit the measured impedance and phase angle. Moreover, the difference in the equivalent circuit models was compared to better understand biological processes that affect neural signal recording.

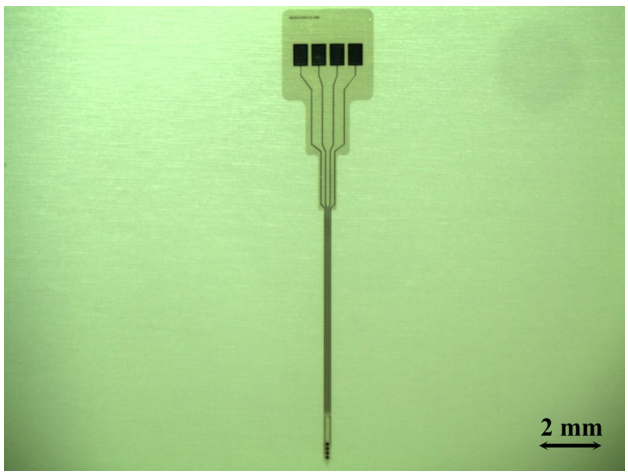

Fig. 1 The profile of the flexible PI-based neural electrode

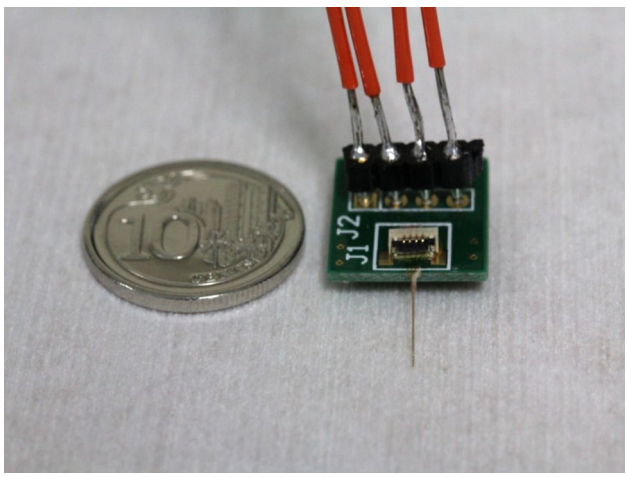

Fig. 2 Optical image of the packaged flexible PI-based neural electrode

2 Materials and methods

2.1 Sample preparation

The flexible polyimide-based gold electrodes used in this study were micro fabricated via standard MEMS processes (Sun et al. 2012; Tsang et al. 2012), and were composed of a sandwich structure of two polyimide (PI) insulating layers (5 μm in thickness for each layer) and an in-between metallization (Ti/Au, 10/250 nm in thickness, respectively). As shown in Fig. 1, the flexible polyimide-based gold microelectrode has four gold recording sites, bonding pad areas, and a single shaft which is 8 mm long, 10 μm thick and 200 μm wide. Each gold recording site is a circle (Ø 90 μm) with a contact area of 6,358.5 μm^2, and electrically connected to a bonding pad. Figure 2 shows the packaged flexible neural electrode. First, the bonding pad area of the electrode was clamped by an FFC\FPC connector (FH 19SC-4S-0.5SH, Hisrose Electric Co. Ltd.) mounted on a printed circuit board (PCB). Electrical wires were then soldered into sockets to connect the potentiostat during EIS measurement.

2.2 Surface characterization and EIS measurement

A field emission scanning electron microscope (FE-SEM, JSM-6700F, JEOL, USA) was used to observe surface morphology of gold recording sites. A standard three-electrode system was used for EIS testing, i.e. the PI-based gold microelectrode was used as the working electrode and the counter electrode was pure platinum. The potential of the working electrode was in reference to an Ag/AgCl electrode. Neural cell culture medium (Gibco® RPMI 1640 Medium, Life Technologies) containing 10 % horse serum (Sigma), 5 % fetal bovine serum (Sigma), were served as the electrolyte to investigate the electrode–cell medium interface. Recoding sites of the flexible PI-based gold microelectrodes ($n = 4$) were immersed in neural cell culture medium for 9 days, and the cell medium was refreshed every 2 days. At day 0, 3, 5, 7 and 9, EIS measure was carried out, using an electrochemical workstation (PGSTA302, Autolab, Switzerland). 50 mV was chosen as the perturbation potential and the frequency range was 0.5×10^{-1} to 1.0×10^{5} Hz. Impedance of the flexible PI-based gold microelectrodes was recorded as a function of frequency of the applied voltage. After EIS measurement at day 9, the PI-based gold microelectrodes were rinsed twice using distilled water and then the surface of recording sites was analyzed using an energy dispersive X-ray (EDX) spectrometer attached to the SEM. In addition, equivalent circuit models, modeled curves and electrochemical parameters were proposed by using the Zview 3.3e impedance analysis software.

3 Results and discussion

Figure 3 displays surface morphology of recoding sites of the flexible PI-based gold microelectrode. The size of the shank and recording sites was identical with the original design, and no defects were observed, such as recording sites delamination, pin holes and cracks in PI insulating layers (Fig. 3a). As shown in the high-magnification SEM image (Fig. 3b), irregularly shaped island structure was formed and uniformly distributed on the surface of the gold recording sites. The island-like morphology is consistent with that of electron-beam evaporated gold thin film in other reports (Chien and Hung 2014; Mtsuko et al. 2008). The average island size measured by ImageJ (National Institutes of Health, USA) was 537.4 ± 357.2 nm. Compared to a smooth gold surface, the surface with the island structure has larger surface area, and therefore lower

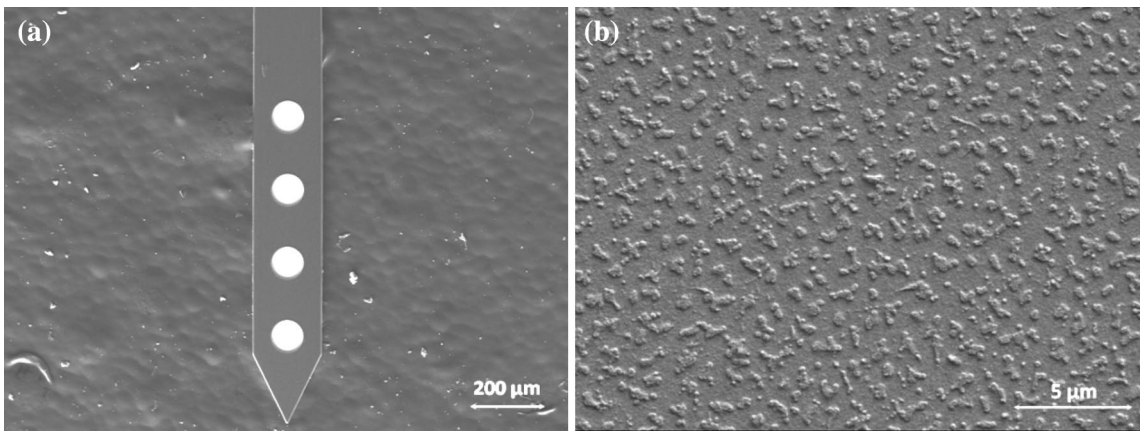

Fig. 3 SEM images of gold recording sites: **a** low magnification, **b** high magnification

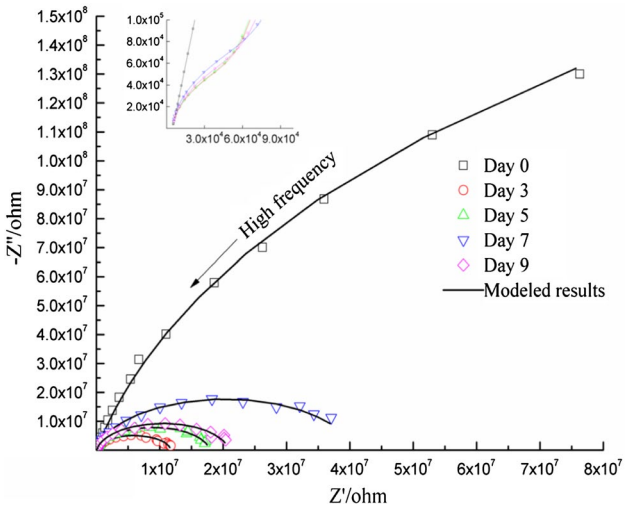

Fig. 4 Nyquist plots of the flexible PI-based gold electrodes immersed in neural cell culture medium at day 0, 3, 5, 7 and 9 days (the *inset* shows higher magnification image of Nyquist plots at low frequency)

impedance. Paik et al. developed a polysilicon substrate roughening process to increase the effective surface area of coated gold recording sites and reduce the interface impedance by a factor of approximate 50 in comparison with a smooth surface (Paik et al. 2003). In addition, Quan et al. found that nano porous gold electrode contributed to a reduced charge transfer resistance due to larger surface to volume ratio (Quan et al. 2011). Moreover, the gold island like structure was reported to enhance electrochemical activity and capacitance of electrode (El-Said et al. 2011).

Figure 4 shows representative Nyquist plots of gold recording sites immersed in cell medium for 0, 3, 5, 7 and 9 days. Nyquist plot describes the frequency response characteristics of the electrode/electrolyte interface as a plot of the real against imaginary component of the impedance, and the frequency increases in a counterclockwise direction in Nyquist plots. At day 0, no obvious semicircle but an arc was present for the microelectrode over the whole frequency range, likely due to the double layer charging and charge transfer of non-ideal planar electrodes as a result of the island-like structure on the electrode surface. After 3 days of immersion, however, the Nyquist plots of the microelectrode exhibited distinct profiles in comparison with that of day 0, and consisted of two semicircles at high and low frequency regions, respectively (the insert in Fig. 4 shows the semicircles at higher frequency region for the electrode immersed for 3, 5, 7 and 9 days). The first semicircle in the high-frequency region arises from the ohmic electrolyte resistance and the impedance resulting from the penetration of the electrolyte through a barrier layer. The second semicircle in the low-frequency region accounts for the processes occurring at electrolyte/electrode interface. In addition, the second depressed semicircle with the theoretical center located below the real axis indicated a surface heterogeneity likely due to protein adsorption processes. The diameter of the semicircles in both high and low frequency regions increased in the order of day 3, 5 and 7, but decreased at day 9. An approximate approach to evaluate the impedance is to compare the diameters of the semicircle in Nyquist plots. The larger the diameter is, the higher impedance exhibits.

Representative Bode plots of impedance modulus and phase angle are shown in Fig. 5a, b, respectively. At day 0 over the whole frequency range, the Bode modulus plot of the recording site exhibited a linear slop of around −0.88 (the impedance of the recording site was inversely proportional to the frequency), indicating that the surface

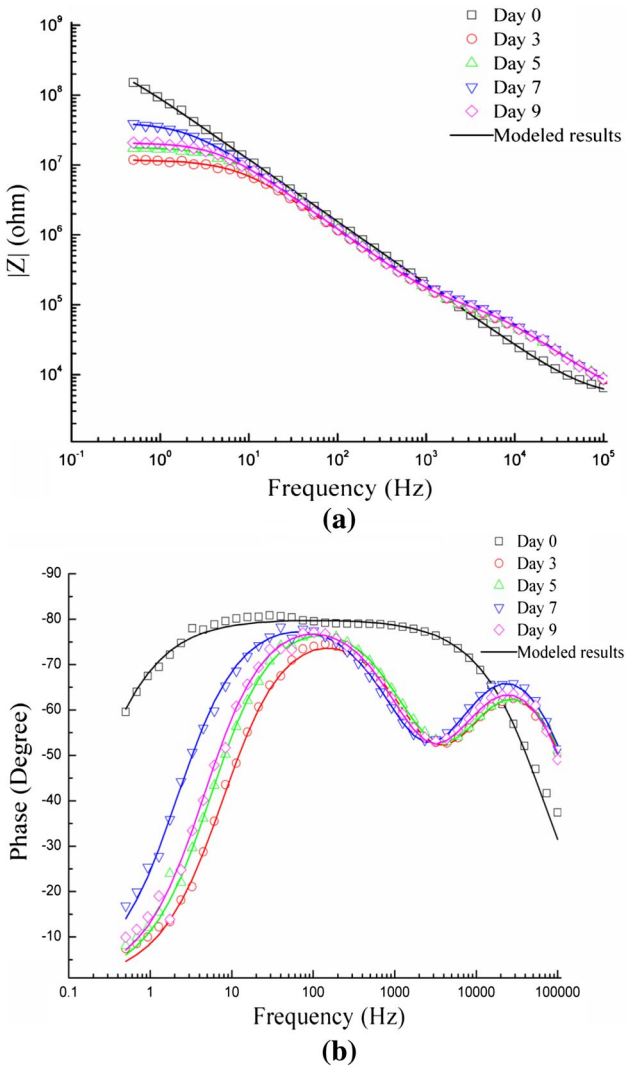

Fig. 5 Representative bode plots of the flexible PI-based gold electrodes immersed in neural cell culture medium at day 0, 3, 5, 7 and 9 days: **a** impedance modulus plot, **b** phase angle plot (modeled results are indicated by the *solid lines*)

of recording sites possessed capacitive characteristics. At day 3, 5, 7 and 9, the impedance of the recording site was higher than that at day 0 in high frequency range (0.5×10^4–1.0×10^5 Hz). In medium frequency range (0.5×10^2 to 0.5×10^4 Hz), however, the impedance of the recording site at day 3–9 was lower than that at day 0, with a slop of around −0.84 to −0.80. Similarly, at low frequencies (0.5–0.5×10^2 Hz) the impedance of recording site at day 3–9 was significantly lower than that at day 0. But the impedance modulus plots of the recording site showed a plateau after 3–9 days of immersion, revealing that the impedance remained stable in this range and was mainly attributed to resistive behaviors.

Phase angle of the recording site (Fig. 5b) started from −35° at day 0 in high frequency range and then gradually shifted to approximately −75° in medium frequency range. A certain degree of deviation from ideal capacitive behavior was recorded in the phase angle plot where the minimum phase angle reached approximately −80° (−10° below −90°) in medium frequency range. Such a deviation was reported by others as well, resulting from surface heterogeneity (Mercanzini et al. 2009). At low frequencies, the phase angle smoothly varied from −80 to −60° for the recording site immersed in cell medium at day 0. In contrast to that of the recording site at day 0, phase angle plots of the recording site at day 3–9 had a similar trend, and showed the presence of two distinct time constants which corresponded to two peaks at high and low frequency ranges in Fig. 5b. The low frequency time constant resulted from the charge transfer processes, whereas the high frequency one could be attributed to the response of the barrier properties of the adsorbed protein layer. Once an implant is inserted into the body, protein adsorption occurs immediately before cells adhere to the surface of the implant. Burgos-Asperilla et al. reported that bovine serum albumin and fetal bovine serum adsorbed on Ti surface after 7 days of immersion acted as a diffusive barrier (Burgos-Asperilla et al. 2010). The study conducted by Selvakumaran et al. showed that after 1 day of exposure to plasma gold surface had around 13 nm thick protein layer (Selvakumaran et al. 2008). However, the equivalent circuit model of the electrode-cell medium interface has not been extensively investigated for the neural microelectrode via EIS.

By means of fitting Nyquist and Bode plots via Zview 3.3e, the electrode-cell medium interface was modeled by equivalent circuit models deriving from Randles model. At day 0, both the Nyquist and Bode plots were fitted well via the Randles equivalent circuit consisting of solution resistance (R_s) in series with a constant phase element (CPE_g) in parallel with the charge transfer resistance (R_{ct}) (Fig. 6a). R_s represents solution resistance measured between working electrode and reference electrode. CPE_g simulates a non-ideal behavior of the capacitor on gold surface due to

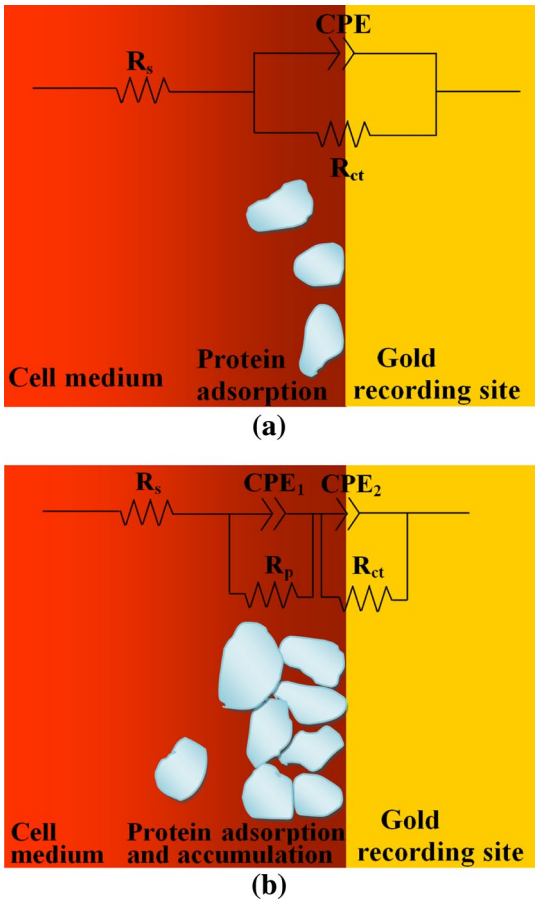

Fig. 6 Equivalent circuit models used for fitting the EIS data of the flexible PI-based gold electrodes immersed in neural cell culture medium: **a** at day 0. **b** day 3, 5, 7 and 9

the surface heterogeneity in structure, topography, etc. R_{ct}, describes the difficulty for charge to transfer between electrode and electrolyte. The lower R_{ct} is, the easier charge can transfer in between. After 3 days of immersion, protein barrier layer was formed on the recording sites due to adsorption and accumulation. To fit Nyquist and Bode plots, R_p and CPE_p in parallel (time constant) were added, corresponding to the resistive and capacitive behaviors of the protein adsorption layer, respectively (Fig. 6b).

Electrochemical parameters of the electrical components in the equivalent circuit models are normalized by the contact area of the recording site, and listed in Table 1. As the distance between the neural microelectrode and reference electrode was maintained at an almost constant level, R_s slightly varied at each time points. R_p was proportional to the thickness of protein adsorption layer, and reached the maximum value at day 7. The decline of R_p at day 9 was likely due to the partial delamination of the protein adsorption layer on gold recording sites, indicating the equilibrium of protein adsorption. The impedance of CPE is defined by Eq. (1) (Mercanzini et al. 2009).

Table 1 Electrochemical parameters of the equivalent circuit models for the electrode at different time points

Time points (day)	R_s (Ω cm^2)	R_{ct} (Ω cm^2)	C_g (μF/cm^2)	n_g	R_p (Ω cm^2)	C_p (μF/cm^2)	n_p
0	$(3.02 \pm 0.06) \times 10^{-3}$	$(2.80 \pm 0.14) \times 10^4$	$(3.29 \pm 0.03) \times 10^1$	0.890 ± 0.001	–	–	–
3	$(2.60 \pm 0.01) \times 10^{-3}$	$(0.75 \pm 0.01) \times 10^3$	$(3.93 \pm 0.07) \times 10^1$	0.905 ± 0.003	3.42 ± 0.11	$(1.65 \pm 0.23) \times 10^1$	0.917 ± 0.012
5	$(2.51 \pm 0.01) \times 10^{-3}$	$(1.14 \pm 0.09) \times 10^3$	$(3.33 \pm 0.06) \times 10^1$	0.921 ± 0.003	3.61 ± 0.12	$(1.85 \pm 0.26) \times 10^1$	0.903 ± 0.013
7	$(2.57 \pm 0.09) \times 10^{-3}$	$(2.72 \pm 0.03) \times 10^3$	$(3.54 \pm 0.05) \times 10^1$	0.915 ± 0.002	4.79 ± 0.13	$(1.54 \pm 0.17) \times 10^1$	0.921 ± 0.010
9	$(2.70 \pm 0.01) \times 10^{-3}$	$(1.33 \pm 0.01) \times 10^3$	$(3.36 \pm 0.73) \times 10^1$	0.925 ± 0.004	4.18 ± 0.17	$(1.73 \pm 0.29) \times 10^1$	0.910 ± 0.015

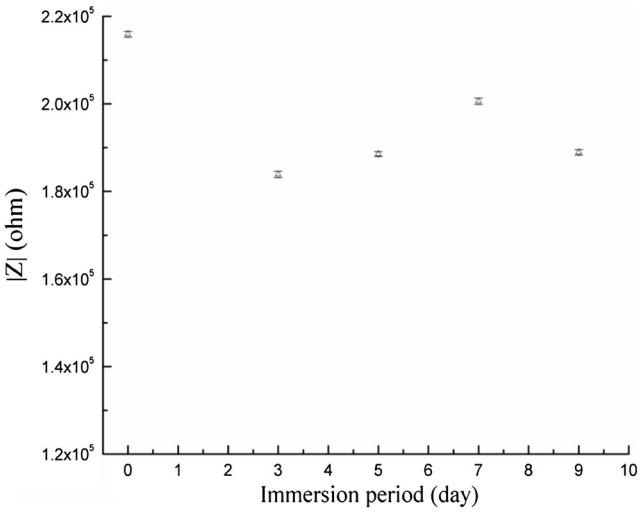

Fig. 7 Impedance of recoding sites immersed in neural cell culture medium at 1 kHz as a function of incubation time

$$Z_{\mathrm{CPE}}(\omega) = \frac{1}{c(\mathrm{j}\omega)^{\mathrm{n}}} \tag{1}$$

CPE is a capacitor as $n = 1$, and a resistor as $n = 0$. Depending on surface roughness, homogeneity, etc., n is determined experimentally. In contrast to R_p, interfacial capacitance of the protein adsorption layer (C_p) was inversely proportional to its thickness and exhibited the minimum value at day 7. R_{ct} was extrapolated from the low frequency data of EIS measurement, resulting from electron–ion charge transfer mechanisms at the electrode surface. Hence, R_{ct} is sensitive to initial electrode–electrolyte conditions (open circuit potential) and applied voltage (Minnikanti et al. 2014). R_{ct} at day 0 can be estimated via Eq. (2) in unit of Ω cm^2 (Mercanzini et al. 2009).

$$R_{\mathrm{ct}} = \frac{V_{\mathrm{t}}}{J_0 z}\left[\frac{e^{\left(\frac{zV_0}{2V_{\mathrm{th}}}\right)}}{2}\right]^{-1} \tag{2}$$

where $V_0 = 50$ mV is the applied amplitude, $V_{th} = 0.0259$ V is thermal voltage, $n_0 = 9.27 \times 10^{25}$ ions/m^3 is bulk concentration of the ion, $z = 4$ is the number of electrons involved in the redox reaction, $J_0 = 0.0398$ A/m^2 is the exchange current density for gold. With these values, R_{ct} calculated by Eq. (2) was 2.16×10^4 Ω cm^2, which is similar to the value (2.80×10^4 Ω cm^2) in Table 1. The variation of R_{ct} at each time point is the same as that of the impedance at 1 kHz and will be discussed in the following section. As proteins adsorbed on the electrode surface and surface area exposed to cell medium reduced, a decline in C_g was expected. On the contrary, C_g rose from 32.90 ± 0.32 μF/cm^2 at day 0–39.30 ± 0.72 μF/cm^2 at day 3, which was likely attributed to the water absorption and penetration of PI layer to

enlarge the contact area. In addition, values of n_g were in agreement with previous reports for neural electrodes (Chan et al. 2009; Minnikanti et al. 2014).

Figure 7 shows the impedance of recoding sites immersed in neural cell culture medium at 1 kHz as a function of incubation time. The frequency of 1 kHz is of great interest for the reason that the duration of action potential of neural cells is close to 1 ms. The impedance of recording sites immersed in neural cell culture medium at day 0 was 215.2 ± 1.2 kΩ at 1 kHz. With the contact area of 85 μm^2, gold recording site of a multielectrode array exhibited the impedance of 6 MΩ at neuron working frequency (1 kHz) in phosphate buffered saline (PBS) (Tsang et al. 2012), while the impedance of a larger gold recording site (1,300 μm^2) reduced to 408 kΩ (Seymour et al. 2011). Additionally, the impedance of a platinum (Pt) recording site with diameter of 50 μm was reported to be 319 kΩ in 0.01 mol/L PBS (Deng et al. 2011). After 3 days of immersion, the impedance of the recording sites decreased by 14.8 % (183.9 kΩ) from day 0, and then remarkably increased to 200.6 kΩ at day 7. Eventually, the impedance stabilized at day 9 (188.9 kΩ) and reduced by 12.5 % from day 0. Tsang et al. also reported the similar trend of impedance variation for the 8 days of immersion in PBS, and impedance reduction of the recording site was less than 10 % (Tsang et al. 2010). In addition, Chen found that the impedance curve of a recording site on a polyimide-based microelectrode array gradually sloped downward into flatness at 1 kHz (Chen et al. 2009). One potential reason for the decrease in impedance is likely due to the water absorption of PI, which in turn increases not only the conductivity of the dielectric material, but also the recording site area exposed to electrolyte (Fig. 8). The water absorption of PI is dependent on its chemical structure, component, sample size, and environment of exposure (temperature, duration and relative humidity. The most possible sites within PI molecular for hydrogen bonding in water are believed to be the ether linkage and the imide carbonyl groups (Demir et al. 2006). It was reported that the water absorption rate of 1-phenyl pyromellitic dianhydride based PI film (5 × 5 mm) was in the range of 2.09–3.26 % after 7 days of immersion in distilled water at 25 °C, while that of PI foil (210 mm × 300 mm × 25 μm) maintained almost constant over time in PBS and varied from 1.1 to 1.46 % (Adhikari et al. 2011). As shown in Fig. 8, water absorption occurring at the junction between the recoding site and PI could enlarge the contact area of the recording sites, resulting in the decreased impedance. Therefore, in the design of next generation of the flexible PI-base neural electrode, waterproofing of the junction between recording site and PI should be considered to minimize the water penetration and elongate the lifetime of the neural electrode.

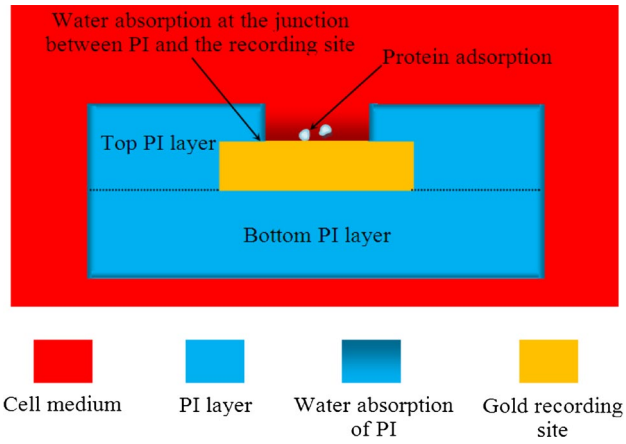

Fig. 8 Schematic diagram of cross sectional view of the flexible PI-based gold electrode immersed in neural cell culture medium (not to the scale)

As reactive tissues resulting from foreign body responses and scar tissues encapsulating neural electrode have higher resistive properties than normal tissue, the impedance of neural electrodes usually increased for weeks following implantation, and then stabilized after tissue remodeling at the electrode interface (Sillay et al. 2013). The 1 kHz magnitude impedance of a Tungsten microwire electrode increased from a range of 75–125 kΩ on the first day to a range of 200–375 kΩ on day 7 (Williams et al. 2007). In addition, a rapid increase in the electrode impedance was recorded over the first 20 days of implantation due to the tissue reaction (Mercanzini et al. 2009). In this in vitro study, the increase in impedance from day 3 was thought to be mainly attributed to protein accumulation on the recording sites. Duan et al. demonstrated the presence of various proteins, bio-films or fibrils on the surface of Pt neural electrode in vivo (Duan et al. 2004). After incubation in bovine serum albumin solution in vitro, the conductivity of polyaniline coated Pt electrode declined from 1.209 × 10^5 to 1.843 × 10^7 Ω/sq (Wang et al. 2010).

Although water absorption and protein adsorption occurred simultaneously during the electrode immersion, water absorption was dominated in the first few days and adsorbed proteins did not significantly affect the impedance due to less accumulation on the surface of recording sites. After 3 days of immersion, however, the PI was saturated, and more proteins accumulated on the surface of recording sites. The adsorbed protein layer had the effect of blocking the electron transfer, resulting in significant positive impact on impedance. Moreover, the equivalent circuit models and fitted parameters of recording sites at different time points revealed the protein adsorption and accumulation process. Therefore, the measured impedance of the recording sites declined first, and then

Table 2 Element concentration on the surface of the recording site before and after immersion

Sample	Surface composition (at%)			
	C	*O*	Au	Ti
Recording site before immersion	5.86	–	93.51	0.63
Recording site after immersion	10.95	1.71	86.8	0.54

increased greatly with immersion time. It was reported that degree of protein adsorption on gold surface was dictated by electrostatic interaction, protein concentration, surface properties, etc. (Jung et al. 2014; Moulton et al. 2003). The thickness of protein layers on a Ti surface was similar after 7 and 28 days exposure to plasma (Selvakumaran et al. 2008), while Moulton et al. showed that the protein adsorption equilibrium was not reached on gold surface until 60 min (Moulton et al. 2003). Moreover, Franks et al. found that the impedance of Pt electrode did not change significantly after 7 days of in vitro immersion in 10 % horse serum solution (Franks et al. 2005). In this study, the flexible polymer-based electrode was immersed in neural cell culture medium for 9 days to mimetic the electrode encapsulation by proteins and investigate the effect of incubation time on the electrical properties of the electrode. On the basis of the electrochemical parameters of the electrical components in the equivalent circuit models, the capacitance of the protein barrier layers was similar at day 5 and day 9 (18.50 ± 2.64 and 17.30 ± 2.86 μF/cm^2, respectively), indicating the saturation of protein adsorption.

In Table 2, the EDX analyses of the recording site revealed that *C* element concentration rose from 5.86 % before the immersion to 10.95 % after the immersion for 9 days. Similarly, the *O* element concentration increased from a nearly undetectable value to 1.71 % at day 9. But the gold element concentration in the detected area reduced from 93.51 % at day 0 to 86.8 % at day 9. The increase of the element concentration for *C* and *O* indicated that a protein layer adsorbed onto the surface of gold recording sites during the immersion in the cell culture medium. As in the microfabrication process Ti layer was prepared via e-beam evaporation below the gold layer to enhance the bonding strength, Ti element was detected in the EDX analyses and its element concentration declined as well due to the protein adsorption.

4 Conclusions

The flexible PI-based gold microelectrode was fabricated and its recording sites exhibited island-like structure which could improve the contact area and reduce the impedance. After being packaged, the microelectrodes were immersed in neural cell culture medium for 9 days to investigate into the microelectrode–cell medium interface. At each time point, EIS measurement was carried out to obtain Nyquist and Bode plots. From day 3, Nyquist and Bode plots of the microelectrode exhibited distinct profiles in comparison with those at day 0, as a result of protein adsorption and accumulation. An equivalent circuit model consisting of two time constants was proposed to describe the protein barrier layer on the gold recording sites, and fit the Nyquist and Bode plots. Although protein accumulation could increase the impedance of the recording sites, the impedance at 1 kHz reduced from 215.9 kΩ (day 0) to 183.9 kΩ after 3 days of immersion in neural cell culture medium, due to water absorption of PI. From day 3 to day 7, PI became saturated and the impedance rose to 200.6 kΩ. Eventually, the impedance stabilized at day 9 due to the combination effects of protein accumulation on recording sites and water adsorption of PI.

Acknowledgments The authors gratefully acknowledge staffs in the Bioelectronics Lab, Institute of Microelectronics for their generous help and valuable suggestions. This work was supported by the Science and Engineering Research Council of Agency for Science, Technology and Research (A*STAR) under Grant 1021710159, and also by Basic Science Research Program through the National Research Foundation of Korea (NRF) funded by the Ministry of Science, ICT and Future Planning (NRF-2013R1A1A1012616).

References

Adhikari R, Dao B, Hodgkin J, Mardel J (2011) Synthesis, structures and membrane properties of siloxane-imide co-polymers produced by aqueous polymerization. Eur Polym J 47(6):1328–1337

Baek DH, Moon JH, Choi YY, Lee M, Choi JH, Pak JJ, Lee SH (2011) A dry release of polyimide electrodes using Kapton film and application to EEG signal measurements. Microsyst Technol 17(1):7–14

Burgos-Asperilla L, García-Alonso MC, Escudero ML, Alonso C (2010) Study of the interaction of inorganic and organic compounds of cell culture medium with a Ti surface. Acta Biomater 6(2):652–661

Chan HY, Aslam DM, Wiler JA, Casey B (2009) A novel diamond microprobe for neuro-chemical and -electrical recording in neural prosthesis. J Microelectromech S 18(3):511–521

Chapin JK, Moxon KA, Markowitz RS, Nicolelis MAL (1999) Real-time control of a robot arm using simultaneously recorded neurons in the motor cortex. Nat Neurosci 2(7):664–670

Chen YY, Lai HY, Lin SH, Cho CW, Chao WH, Liao CH, Lin SY (2009) Design and fabrication of a polyimide-based microelectrode array: application in neural recording and repeatable electrolytic lesion in rat brain. J Neurosci Meth 182(1):6–16

Chien TM, Hung WH (2014) Observation of strong plasmonic heating in Au-Fe_2O_3 nanocomposite. Mater Express 1(1):015009

Collinger JL, Wodlinger BD, John E, Wang W, Tyler-Kabara EC, Weber DJ, Schwartz AB (2013) High-performance neuroprosthetic control by an individual with tetraplegia. Lancet 381(9866):557–564

Demir H, Atikler U, Balköse D, Tıhmınlıoğlu F (2006) The effect of fiber surface treatments on the tensile and water sorption properties of polypropylene–luffa fiber composites. Compos Part A Appl S 37(3):447–456

Deng M, Yang X, Silke M, Qiu W, Xu M, Borghs G, Chen H (2011) Electrochemical deposition of polypyrrole/graphene oxide composite on microelectrodes towards tuning the electrochemical properties of neural probes. Sens Actuators B 158(1):176–184

Duan YY, Clark GM, Cowan RSC (2004) A study of intra-cochlear electrodes and tissue interface by electrochemical impedance methods in vivo. Biomaterials 25(17):3813–3828

El-Said WA, Lee JH, Oh BK, Choi JW (2011) Electrochemical sensor to detect neurotransmitter using gold nano-island coated ITO electrode. J Nanosci Nanotechnol 11(7):6539–6543

Franks W, Schenker I, Schmutz P, Hierlemann A (2005) Impedance characterization and modeling of electrodes for biomedical applications. IEEE Trans Biomed Eng 52(7):1295–1302

Gilletti A, Muthuswamy J (2006) Brain micromotion around implants in the rodent somatosensory cortex. J Neural Eng 3(3):189

Jung N, Kim D, Yim C, Park JY, Chang BY, Jeon S (2014) Quartz resonator for simultaneous measurement of changes in mass and electrical impedance during protein adsorption. J Electrochem Soc 161(2):B3107–B3110

Mercanzini A, Colin P, Bensadoun JC, Bertsch A, Renaud P (2009) In vivo electrical impedance spectroscopy of tissue reaction to microelectrode arrays. IEEE Trans Biomed Eng 56(7):1909–1918

Minnikanti S, Diao G, Pancrazio JJ, Xie X, Rieth L, Solzbacher F, Peixoto N (2014) Lifetime assessment of atomic-layer-deposited Al_2O_3–Parylene C bilayer coating for neural interfaces using accelerated age testing and electrochemical characterization. Acta Biomater 10(2):960–967

Moulton SE, Barisci JN, Bath A, Stella R, Wallace GG (2003) Investigation of protein adsorption and electrochemical behavior at a gold electrode. J Colloid Interf Sci 261(2):312–319

Mtsuko D, Avnon A, Lievonen J, Ahlskog M, Menon R (2008) Electrochemical deposition of polypyrrole nanolayers on discontinuous ultrathin gold films. Nanotechnology 19(12):125304

Paik SJ, Park Y, Cho DD (2003) Roughened polysilicon for low impedance microelectrodes in neural probes. J Micromech Microeng 13(3):373

Quan X, Fischer LM, Boisen A, Tenje M (2011) Development of nanoporous gold electrodes for electrochemical applications. Microelectron Eng 88(8):2379–2382

Rousche PJ, Normann RA (1998) Chronic recording capability of the utah intracortical electrode array in cat sensory cortex. J Neurosci Meth 82(1):1–15

Rui Y, Liu J, Wang Y, Yang C (2011) Parylene-based implantable Pt-black coated flexible 3-D hemispherical microelectrode arrays for improved neural interfaces. Microsyst Technol 17(3):437–442

Selvakumaran J, Keddie J, Ewins D, Hughes MP (2008) Protein adsorption on materials for recording sites on implantable microelectrodes. J Mater Sci Mater Med 19(1):143–151

Seymour JP, Langhals NB, Anderson DJ, Kipke DR (2011) Novel multi-sided, microelectrode arrays for implantable neural applications. Biomed Microdevices 13(3):441–451

Shanechi MM, Hu RC, Williams ZM (2014) A cortical–spinal prosthesis for targeted limb movement in paralysed primate avatars. Nat Commun 5:3237

Sillay KA, Rutecki P, Cicora K, Worrell G, Drazkowski J, Shih JJ, Sharan AD, Morrel MJ, Williams J, Wingeier B (2013) Long-term measurement of impedance in chronically implanted depth and subdural electrodes during responsive neurostimulation in humans. Brain Stimul 6(5):718–726

Sun T, Park WT, Cheng MY, An JZ, Xue RF, Tan KL, Je M (2012) Implantable polyimide cable for multichannel high-data-rate neural recording microsystems. IEEE Trans Biomed Eng 59(2):390–399

Tsang WM, Stone AL, Aldworth ZN, Hildebrand JG, Daniel TL, Akinwande AI, Voldman J (2010) Flexible split-ring electrode for insect flight biasing using multisite neural stimulation. IEEE Trans Biomed Eng 57(7):1757–1764

Tsang WM, Stone AL, Otten D, Aldworth ZN, Daniel TL, Hildebrand JG, Levine RB, Voldman J (2012) Insect-machine interface: a carbon nanotube-enhanced flexible neural probe. J Neurosci Meth 204(2):355–365

Wang LP, Wang W, Di L, Lu YN, Wang JY (2010) Protein adsorption under electrical stimulation of neural probe coated with polyaniline. J Colloid Interf Sci 80(1):72–78

Williams JC, Hippensteel JA, Dilgen J, Shain W, Kipke DR (2007) Complex impedance spectroscopy for monitoring tissue responses to inserted neural implants. J Neural Eng 4(4):410–423